

Measurement of the effective b quark fragmentation function at the Z resonance

D. Buskulic, D. Casper, I. de Bonis, D. Decamp, P. Ghez, C. Goy, J.P. Lees, A. Lucotte, M.N. Minard, P. Odier, et al.

▶ **To cite this version:**

D. Buskulic, D. Casper, I. de Bonis, D. Decamp, P. Ghez, et al.. Measurement of the effective b quark fragmentation function at the Z resonance. Physics Letters B, 1995, 357, pp.699-714. in2p3-00002081

HAL Id: in2p3-00002081
https://hal.in2p3.fr/in2p3-00002081

Submitted on 17 May 1999

HAL is a multi-disciplinary open access archive for the deposit and dissemination of scientific research documents, whether they are published or not. The documents may come from teaching and research institutions in France or abroad, or from public or private research centers.

L'archive ouverte pluridisciplinaire **HAL**, est destinée au dépôt et à la diffusion de documents scientifiques de niveau recherche, publiés ou non, émanant des établissements d'enseignement et de recherche français ou étrangers, des laboratoires publics ou privés.

EUROPEAN LABORATORY FOR PARTICLE PHYSICS (CERN)

CERN–PPE/95–113
20 July 1995

Measurement of the effective b quark fragmentation function at the Z resonance

The ALEPH Collaboration [1]

Abstract

Using a sample of about 1.46 million hadronic Z decays collected between 1991 and 1993 with the ALEPH detector at LEP, the energy distribution of the B^0 and $B^{\pm}$ mesons produced at the Z resonance is measured by reconstructing semileptonic decays $B\rightarrow \ell\nu_\ell D(X)$ or $B\rightarrow \ell\nu_\ell D^{*+}(X)$. The charmed mesons are reconstructed through the decay modes $D^0 \rightarrow K^-\pi^+$, $D^0 \rightarrow K^-\pi^+\pi^-\pi^+$, $D^+ \rightarrow K^-\pi^+\pi^+$ and $D^{*+} \rightarrow D^0\pi^+$. The neutrino energy is estimated from the missing energy in the lepton hemisphere. Accounting for B^* and B^{**} production, the shape of the scaled energy distribution $x_E^{(b)}$ for mesons containing a b quark is compared to the predictions of different fragmentation models. The mean value of $x_E^{(b)}$ is found to be

$$\langle x_E^{(b)} \rangle = 0.715 \pm 0.007(\text{stat}) \pm 0.013(\text{syst}).$$

(Submitted to Physics Letters B)

[1] See next pages for the list of authors

The ALEPH Collaboration

D. Buskulic, D. Casper, I. De Bonis, D. Decamp, P. Ghez, C. Goy, J.-P. Lees, A. Lucotte, M.-N. Minard, P. Odier, B. Pietrzyk

Laboratoire de Physique des Particules (LAPP), IN^{2}P^3-CNRS, 74019 Annecy-le-Vieux Cedex, France

F. Ariztizabal, M. Chmeissani, J.M. Crespo, I. Efthymiopoulos, E. Fernandez, M. Fernandez-Bosman, V. Gaitan, Ll. Garrido,[15] M. Martinez, S. Orteu, A. Pacheco, C. Padilla, F. Palla, A. Pascual, J.A. Perlas, F. Sanchez, F. Teubert

Institut de Fisica d'Altes Energies, Universitat Autonoma de Barcelona, 08193 Bellaterra (Barcelona), Spain[7]

A. Colaleo, D. Creanza, M. de Palma, A. Farilla, G. Gelao, M. Girone, G. Iaselli, G. Maggi,[3] M. Maggi, N. Marinelli, S. Natali, S. Nuzzo, A. Ranieri, G. Raso, F. Romano, F. Ruggieri, G. Selvaggi, L. Silvestris, P. Tempesta, G. Zito

Dipartimento di Fisica, INFN Sezione di Bari, 70126 Bari, Italy

X. Huang, J. Lin, Q. Ouyang, T. Wang, Y. Xie, R. Xu, S. Xue, J. Zhang, L. Zhang, W. Zhao

Institute of High-Energy Physics, Academia Sinica, Beijing, The People's Republic of China[8]

G. Bonvicini, M. Cattaneo, P. Comas, P. Coyle, H. Drevermann, A. Engelhardt, R.W. Forty, M. Frank, R. Hagelberg, J. Harvey, R. Jacobsen,[24] P. Janot, B. Jost, J. Knobloch, I. Lehraus, C. Markou,[23] E.B. Martin, P. Mato, H. Meinhard, A. Minten, R. Miquel, T. Oest, P. Palazzi, J.R. Pater,[27] J.-F. Pusztaszeri, F. Ranjard, P. Rensing, L. Rolandi, D. Schlatter, M. Schmelling, O. Schneider, W. Tejessy, I.R. Tomalin, A. Venturi, H. Wachsmuth, W. Wiedenmann, T. Wildish, W. Witzeling, J. Wotschack

European Laboratory for Particle Physics (CERN), 1211 Geneva 23, Switzerland

Z. Ajaltouni, M. Bardadin-Otwinowska,[2] A. Barres, C. Boyer, A. Falvard, P. Gay, C. Guicheney, P. Henrard, J. Jousset, B. Michel, S. Monteil, J-C. Montret, D. Pallin, P. Perret, F. Podlyski, J. Proriol, J.-M. Rossignol, F. Saadi

Laboratoire de Physique Corpusculaire, Université Blaise Pascal, IN^{2}P^3-CNRS, Clermont-Ferrand, 63177 Aubière, France

T. Fearnley, J.B. Hansen, J.D. Hansen, J.R. Hansen, P.H. Hansen, B.S. Nilsson

Niels Bohr Institute, 2100 Copenhagen, Denmark[9]

A. Kyriakis, E. Simopoulou, I. Siotis, A. Vayaki, K. Zachariadou

Nuclear Research Center Demokritos (NRCD), Athens, Greece

A. Blondel,[21] G. Bonneaud, J.C. Brient, P. Bourdon, L. Passalacqua, A. Rougé, M. Rumpf, R. Tanaka, A. Valassi,[31] M. Verderi, H. Videau

Laboratoire de Physique Nucléaire et des Hautes Energies, Ecole Polytechnique, IN^{2}P^3-CNRS, 91128 Palaiseau Cedex, France

D.J. Candlin, M.I. Parsons

Department of Physics, University of Edinburgh, Edinburgh EH9 3JZ, United Kingdom[10]

E. Focardi, G. Parrini

Dipartimento di Fisica, Università di Firenze, INFN Sezione di Firenze, 50125 Firenze, Italy

M. Corden, M. Delfino,[12] C. Georgiopoulos, D.E. Jaffe

Supercomputer Computations Research Institute, Florida State University, Tallahassee, FL 32306-4052, USA [13,14]

A. Antonelli, G. Bencivenni, G. Bologna,[4] F. Bossi, P. Campana, G. Capon, V. Chiarella, G. Felici, P. Laurelli, G. Mannocchi,[5] F. Murtas, G.P. Murtas, M. Pepe-Altarelli

Laboratori Nazionali dell'INFN (LNF-INFN), 00044 Frascati, Italy

S.J. Dorris, A.W. Halley, I. ten Have,[6] I.G. Knowles, J.G. Lynch, W.T. Morton, V. O'Shea, C. Raine, P. Reeves, J.M. Scarr, K. Smith, M.G. Smith, A.S. Thompson, F. Thomson, S. Thorn, R.M. Turnbull

Department of Physics and Astronomy, University of Glasgow, Glasgow G12 8QQ,United Kingdom[10]

U. Becker, O. Braun, C. Geweniger, G. Graefe, P. Hanke, V. Hepp, E.E. Kluge, A. Putzer, B. Rensch, M. Schmidt, J. Sommer, H. Stenzel, K. Tittel, S. Werner, M. Wunsch

Institut für Hochenergiephysik, Universität Heidelberg, 69120 Heidelberg, Fed. Rep. of Germany[16]

R. Beuselinck, D.M. Binnie, W. Cameron, D.J. Colling, P.J. Dornan, N. Konstantinidis, L. Moneta, A. Moutoussi, J. Nash, G. San Martin, J.K. Sedgbeer, A.M. Stacey

Department of Physics, Imperial College, London SW7 2BZ, United Kingdom[10]

G. Dissertori, P. Girtler, E. Kneringer, D. Kuhn, G. Rudolph

Institut für Experimentalphysik, Universität Innsbruck, 6020 Innsbruck, Austria[18]

C.K. Bowdery, T.J. Brodbeck, P. Colrain, G. Crawford, A.J. Finch, F. Foster, G. Hughes, T. Sloan, E.P. Whelan, M.I. Williams

Department of Physics, University of Lancaster, Lancaster LA1 4YB, United Kingdom[10]

A. Galla, A.M. Greene, K. Kleinknecht, G. Quast, J. Raab, B. Renk, H.-G. Sander, R. Wanke, C. Zeitnitz

Institut für Physik, Universität Mainz, 55099 Mainz, Fed. Rep. of Germany[16]

J.J. Aubert, A.M. Bencheikh, C. Benchouk, A. Bonissent,[21] G. Bujosa, D. Calvet, J. Carr, C. Diaconu, F. Etienne, M. Thulasidas, D. Nicod, P. Payre, D. Rousseau, M. Talby

Centre de Physique des Particules, Faculté des Sciences de Luminy, IN^{2}P^3-CNRS, 13288 Marseille, France

I. Abt, R. Assmann, C. Bauer, W. Blum, D. Brown,[24] H. Dietl, F. Dydak,[21] G. Ganis, C. Gotzhein, K. Jakobs, H. Kroha, G. Lütjens, G. Lutz, W. Männer, H.-G. Moser, R. Richter, A. Rosado-Schlosser, S. Schael, R. Settles, H. Seywerd, U. Stierlin,[2] R. St. Denis, G. Wolf

Max-Planck-Institut für Physik, Werner-Heisenberg-Institut, 80805 München, Fed. Rep. of Germany[16]

R. Alemany, J. Boucrot, O. Callot, A. Cordier, F. Courault, M. Davier, L. Duflot, J.-F. Grivaz, Ph. Heusse, M. Jacquet, D.W. Kim,[19] F. Le Diberder, J. Lefrançois, A.-M. Lutz, G. Musolino, I. Nikolic, H.J. Park, I.C. Park, M.-H. Schune, S. Simion, J.-J. Veillet, I. Videau

Laboratoire de l'Accélérateur Linéaire, Université de Paris-Sud, IN^{2}P^3-CNRS, 91405 Orsay Cedex, France

D. Abbaneo, P. Azzurri, G. Bagliesi, G. Batignani, S. Bettarini, C. Bozzi, G. Calderini, M. Carpinelli, M.A. Ciocci, V. Ciulli, R. Dell'Orso, R. Fantechi, I. Ferrante, L. Foà,[1] F. Forti, A. Giassi, M.A. Giorgi, A. Gregorio, F. Ligabue, A. Lusiani, P.S. Marrocchesi, A. Messineo, G. Rizzo, G. Sanguinetti, A. Sciabà, P. Spagnolo, J. Steinberger, R. Tenchini, G. Tonelli,[26] G. Triggiani, C. Vannini, P.G. Verdini, J. Walsh

Dipartimento di Fisica dell'Università, INFN Sezione di Pisa, e Scuola Normale Superiore, 56010 Pisa, Italy

A.P. Betteridge, G.A. Blair, L.M. Bryant, F. Cerutti, Y. Gao, M.G. Green, D.L. Johnson, T. Medcalf, Ll.M. Mir, P. Perrodo, J.A. Strong

Department of Physics, Royal Holloway & Bedford New College, University of London, Surrey TW20 OEX, United Kingdom[10]

V. Bertin, D.R. Botterill, R.W. Clifft, T.R. Edgecock, S. Haywood, M. Edwards, P. Maley, P.R. Norton, J.C. Thompson

Particle Physics Dept., Rutherford Appleton Laboratory, Chilton, Didcot, Oxon OX11 OQX, United Kingdom[10]

B. Bloch-Devaux, P. Colas, H. Duarte, S. Emery, W. Kozanecki, E. Lançon, M.C. Lemaire, E. Locci, B. Marx, P. Perez, J. Rander, J.-F. Renardy, A. Rosowsky, A. Roussarie, J.-P. Schuller, J. Schwindling, D. Si Mohand, A. Trabelsi, B. Vallage

CEA, DAPNIA/Service de Physique des Particules, CE-Saclay, 91191 Gif-sur-Yvette Cedex, France[17]

R.P. Johnson, H.Y. Kim, A.M. Litke, M.A. McNeil, G. Taylor

Institute for Particle Physics, University of California at Santa Cruz, Santa Cruz, CA 95064, USA[22]

A. Beddall, C.N. Booth, R. Boswell, S. Cartwright, F. Combley, I. Dawson, A. Koksal, M. Letho, W.M. Newton, C. Rankin, L.F. Thompson

Department of Physics, University of Sheffield, Sheffield S3 7RH, United Kingdom[10]

A. Böhrer, S. Brandt, G. Cowan, E. Feigl, C. Grupen, G. Lutters, J. Minguet-Rodriguez, F. Rivera,[25] P. Saraiva, L. Smolik, F. Stephan, P. van Gemmeren

Fachbereich Physik, Universität Siegen, 57068 Siegen, Fed. Rep. of Germany[16]

M. Apollonio, L. Bosisio, R. Della Marina, G. Giannini, B. Gobbo, F. Ragusa[20]

Dipartimento di Fisica, Università di Trieste e INFN Sezione di Trieste, 34127 Trieste, Italy

J. Rothberg, S. Wasserbaech

Experimental Elementary Particle Physics, University of Washington, WA 98195 Seattle, U.S.A.

S.R. Armstrong, L. Bellantoni,[30] P. Elmer, Z. Feng, D.P.S. Ferguson, Y.S. Gao, S. González, J. Grahl, J.L. Harton,[28] O.J. Hayes, H. Hu, P.A. McNamara III, J.M. Nachtman, W. Orejudos, Y.B. Pan, Y. Saadi, M. Schmitt, I.J. Scott, V. Sharma,[29] J.D. Turk, A.M. Walsh, Sau Lan Wu, X. Wu, J.M. Yamartino, M. Zheng, G. Zobernig

Department of Physics, University of Wisconsin, Madison, WI 53706, USA[11]

[1] Now at CERN, 1211 Geneva 23, Switzerland.
[2] Deceased.
[3] Now at Dipartimento di Fisica, Università di Lecce, 73100 Lecce, Italy.
[4] Also Istituto di Fisica Generale, Università di Torino, Torino, Italy.
[5] Also Istituto di Cosmo-Geofisica del C.N.R., Torino, Italy.
[6] Now at TSM Business School, Enschede, The Netherlands.
[7] Supported by CICYT, Spain.
[8] Supported by the National Science Foundation of China.
[9] Supported by the Danish Natural Science Research Council.
[10] Supported by the UK Particle Physics and Astronomy Research Council.
[11] Supported by the US Department of Energy, grant DE-FG0295-ER40896.
[12] On leave from Universitat Autonoma de Barcelona, Barcelona, Spain.
[13] Supported by the US Department of Energy, contract DE-FG05-92ER40742.
[14] Supported by the US Department of Energy, contract DE-FC05-85ER250000.
[15] Permanent address: Universitat de Barcelona, 08208 Barcelona, Spain.
[16] Supported by the Bundesministerium für Forschung und Technologie, Fed. Rep. of Germany.
[17] Supported by the Direction des Sciences de la Matière, C.E.A.
[18] Supported by Fonds zur Förderung der wissenschaftlichen Forschung, Austria.
[19] Permanent address: Kangnung National University, Kangnung, Korea.
[20] Now at Dipartimento di Fisica, Università di Milano, Milano, Italy.
[21] Also at CERN, 1211 Geneva 23, Switzerland.
[22] Supported by the US Department of Energy, grant DE-FG03-92ER40689.
[23] Now at University of Athens, 157-71 Athens, Greece.
[24] Now at Lawrence Berkeley Laboratory, Berkeley, CA 94720, USA.
[25] Partially supported by Colciencias, Colombia.
[26] Also at Istituto di Matematica e Fisica, Università di Sassari, Sassari, Italy.
[27] Now at Schuster Laboratory, University of Manchester, Manchester M13 9PL, UK.
[28] Now at Colorado State University, Fort Collins, CO 80523, USA.
[29] Now at University of California at San Diego, La Jolla, CA 92093, USA.
[30] Now at Fermi National Accelerator Laboratory, Batavia, IL 60510, USA.
[31] Supported by the Commission of the European Communities, contract ERBCHBICT941234.

1 Introduction

The measurement of the energy spectra of heavy flavour hadrons produced in Z decays tests the hadronization mechanism of heavy quarks into physical states, but also has practical importance for many b physics measurements at LEP. The predicted B hadron energy distributions depend upon a convolution of perturbative QCD (i.e. hard gluon radiation) and the hadronization mechanism itself. Due to the non-perturbative nature of the latter, precise quantitative predictions are still missing, and phenomenological models must be used to describe the hadronization process.

Assuming that the transition amplitude for a fast moving heavy quark Q to fragment into a hadron $\mathrm{H} = (\mathrm{Q}\bar{\mathrm{q}})$ and a light quark q is proportional to the inverse of the energy transfer $\Delta E^{-1} = (E_{\mathrm{H}} + E_{\mathrm{q}} - E_{\mathrm{Q}})^{-1}$ in the breakup process, the following parametrization has been proposed by Peterson et al. [1] for heavy quark fragmentation:

$$D_{\mathrm{Q}}^{H}(z) \propto \frac{1}{z}\left(1 - \frac{1}{z} - \frac{\epsilon_{\mathrm{Q}}}{1-z}\right)^{-2}. \tag{1}$$

Although other forms of the fragmentation function have been suggested in the literature [2, 3, 4], the shape of Ref. [1] is widely used in the interpretation of experimental results and in the modelling of b-hadron production in simulation programs. The only parameter of the model, ϵ_{Q}, is expected to be the squared ratio of the effective light quark mass to the heavy quark mass

$$\epsilon_{\mathrm{Q}} \approx \frac{m_{\mathrm{q}}^2}{m_{\mathrm{Q}}^2}, \tag{2}$$

and z is defined as

$$z = \frac{(E + p_{\parallel})_{hadron}}{(E+p)_{quark}}. \tag{3}$$

Here, $(E+p)_{quark}$ is the sum of the energy and momentum of the quark after accounting for initial state radiation, gluon bremsstrahlung and photon radiation in the final state. Unfortunately, this variable is not experimentally accessible on an event-by-event basis and the interpretation of the results in terms of z can therefore only be given in the context of a specific model. Results are usually expressed in terms of the scaled energy x_E, defined as the ratio of the heavy hadron energy to the beam energy

$$x_E = \frac{E_{hadron}}{E_{beam}}. \tag{4}$$

This variable, which includes the effect of photon and hard gluon radiation, is used in the present analysis.

To date, the b-quark fragmentation function at the Z peak has mostly been probed indirectly by studies of inclusive lepton spectra in b semileptonic decays [5, 6, 7, 8], by inclusive J/ψ production [9] and by charged particle multiplicities in $\mathrm{Z} \to \mathrm{b\bar{b}}$ events [10]. Such measurements usually only provide information about the mean energy fraction $\langle x_E \rangle$ carried by the b flavoured

hadrons, although some attempts have been made to unfold the shape of the x_E distributions from the lepton momentum spectra [7].

Another promising method [11] uses semileptonic B meson decays $B \to \ell\nu_\ell D(X)$ with full reconstruction of the D meson, computing the missing neutrino energy from energy-momentum conservation. It has the advantage of directly measuring the B energy spectrum, independently of the fragmentation model, but has been limited, until now, by the small number of events available.

This paper presents a new measurement of the b-quark fragmentation using about 1400 decays $B \to \ell\nu_\ell D(X)$ reconstructed with the ALEPH detector at LEP. It is based on a data sample of about 1.465 million hadronic Z decays collected between 1991 and 1993. The symbol B represents either a B^0_d or a $B^\pm$ meson. The symbol D represents any fully reconstructed charmed meson and can be either a D^0, a $D^\pm$ or a $D^{*\pm}$. The following charmed meson decay channels have been used in the analysis: $D^0 \to K^-\pi^+$, $K^-\pi^+\pi^-\pi^+$, $D^+ \to K^-\pi^+\pi^+$ and $D^{*+} \to D^0\,\pi^+$ followed by $D^0 \to K^-\pi^+$ or $K^-\pi^+\pi^-\pi^+$. The symbol X represents all particles which are not explicitly identified as originating from the B decay. It can be either a π^0 (γ) from the decay $B \to \ell\nu_\ell$ D^{*0} with $D^{*0} \to D^0\,\pi^0$ (γ) or an additional π produced in the decay $B \to \ell\nu_\ell D^{**}$. Here D^{**} is a generic term covering all the non-resonant decays to $D^{(*)} + n\pi$ or decays to P-wave charmed mesons and higher spin states decaying to $D^{(*)}\pi$; unless otherwise specified, a mixture of 50% narrow resonant and 50% non-resonant or wide resonant states are called D^{**} throughout the paper.

The outline of this paper is as follows. First, a brief description of the ALEPH experiment is presented. The selection of $B \to \ell\nu_\ell D(X)$ events is described in Section 3. The measurement of the B momentum using neutrino energy reconstruction is discussed in Section 4. Section 5 is devoted to the study of b fragmentation, and Section 6 describes the main systematic errors affecting this measurement.

While the reconstructed particles are either B^0_d or $B^\pm$ mesons, the quantity relevant for the study of the b fragmentation is the scaled energy of the first b-hadron produced in the b-quark hadronization. For B^0_d or $B^\pm$ states, the first b-hadron can be either a B, a B^* or an orbitally excited B^{**} state. For clarity, throughout the paper $x_E^{(B)}$ denotes the scaled energy of the B^0_d or $B^\pm$ meson, and $x_E^{(b)}$ the scaled energy of the first B, B^* or B^{**} state. The first b-hadron produced in b quark hadronization is called the leading b-hadron. A comparison of the $x_E^{(B)}$ distribution to the predictions of different fragmentation models and a reconstruction of the $x_E^{(b)}$ spectrum after corrections for acceptance, detector resolution and missing particles are given in Section 5.

2 Detector description and lepton identification

A detailed description of the ALEPH detector and of its performance can be found in Ref. [12, 13]. The charged particles are tracked inside a three-component magnetic spectrometer

immersed in the 1.5 T field from a superconducting solenoid. Closest to the beam pipe is the vertex detector (VDET) [16], consisting of double sided silicon microstrip detectors, arranged in two cylindrical layers at average radii of 6.3 and 10.8 cm. This detector covers an angular range $|\cos\theta| \leq 0.85$ for the inner layer, and $|\cos\theta| \leq 0.69$ for the outer layer. The spatial resolution for $r\phi$ coordinates is 12 μm; for z coordinates, it varies between 12 and 22 μm, depending on the polar angle of the charged particle. The vertex detector is surrounded by a drift chamber (ITC) with eight axial wire layers up to a radius of 26 cm, and a time projection chamber (TPC) which measures up to 21 three dimensional space points per track at radii between 40 and 171 cm. With this combined system, a transverse momentum resolution $\sigma(1/p_T) = 0.6 \times 10^{-3}(\mathrm{GeV/c})^{-1}$ is achieved. For tracks with associated hits in both layers of the VDET, the impact parameter resolution is $\sigma = 25\mu\mathrm{m} + 95\mu\mathrm{m/p}$ (p in GeV/c), in both the $r\phi$ and the z views. The tracking system allows the interaction point to be reconstructed on an event-by-event basis [17, 18], with an average resolution of 85μm for $\mathrm{b\bar{b}}$ events.

The TPC also provides up to 338 measurements of the specific ionization for charged particles, allowing electrons to be separated from other charged particle species by more than three standard deviations up to a momentum of 8 GeV/c. In the relativistic rise region, the $\pi - \mathrm{K}$ separation is roughly two standard deviations.

The electromagnetic calorimeter (ECAL) is a lead-proportional chamber sandwich with cathode pad readout in $0.9^0 \times 0.9^0$ projective towers with three segments in depth. Electrons, as well as photons, are identified by the characteristic longitudinal and transverse developments of their associated showers.

Muons are identified by their characteristic penetration pattern in the hadron calorimeter (HCAL) and in the muon chambers. The HCAL is the iron return yoke of the magnet, instrumented with 23 layers of streamer tubes which provide a two dimensional measurement of muon tracks and of the hadronic shower development. The muon chambers surround the HCAL and consist of two double layers of streamer tubes, providing three dimensional information on the position of each hit.

The total visible energy is measured with an energy-flow reconstruction algorithm [13] which combines all the above measurements and gives a relative resolution of $0.60/\sqrt{E}$ (E in GeV) on the total visible energy for hadronic Z decays. This algorithm, which also provides a list of charged and neutral reconstructed objects, is used in the following analysis to compute the visible energy in the b-hadron hemisphere.

3 Selection of $\mathrm{B} \to \ell\nu_\ell\mathrm{D(X)}$ events

The decays $\mathrm{B} \to \ell\nu_\ell\mathrm{D(X)}$ are searched for in hadronic events [14] containing at least one identified lepton of momentum $p > 3$ GeV/c. Leptons are identified using the standard criteria of Ref. [14]. The transverse momentum p_T of the lepton with respect to the closest jet is computed as described in [14], where the jets are built using the JADE algorithm [15] with

$y_{cut} = (6\ \mathrm{GeV}/\sqrt{s})^2$ and where the lepton is excluded from the jet for the p_T definition. A cut $p_T > 1$ GeV/c is applied to reject background from non-primary b decays.

Events are divided into two hemispheres with respect to a plane perpendicular to the thrust axis. The D and D* meson decays are reconstructed in the five decay channels $\mathrm{D}^0 \to \mathrm{K}\pi, \mathrm{K}\pi\pi\pi$, $\mathrm{D}^\pm \to \mathrm{K}\pi\pi$ and $\mathrm{D}^{*\pm} \to \mathrm{D}^0\pi^\pm$ with $\mathrm{D}^0 \to \mathrm{K}\pi, \mathrm{K}\pi\pi\pi$, by combining tracks within the lepton hemisphere. In all the decay channels, the D momentum is required to exceed 5 GeV/c to reduce the combinatorial background, except for the channel $\mathrm{D}^{*\pm} \to \mathrm{D}^0\pi^\pm(\mathrm{D}^0 \to \mathrm{K}\pi)$ where this cut is lowered to 3 GeV/c to improve the efficiency at small $x_E^{(\mathrm{b})}$.

Charged kaon candidates must have the same charge as the lepton, as expected for a semileptonic B decay. If the dE/dx measurement is available ($\sim 90\%$ of the tracks), the ionization of the $\mathrm{K}^\pm$ must be within two standard deviations of the expected value. For all the decay modes, a cut $p_\mathrm{K} > 1.5$ GeV/c is applied to the charged kaon momentum. The most energetic pion must have a momentum $p_\pi > 1$ GeV/c and the others (for $\mathrm{K}\pi\pi\pi$ and $\mathrm{K}\pi\pi$ decays) are required to satisfy $p_\pi > 0.5$ GeV/c.

In the $\mathrm{K}\pi$ and $\mathrm{K}\pi\pi\pi$ channels, $\mathrm{D}^{*\pm}$ decaying to $\mathrm{D}^0\ \pi^\pm$ are identified by combining a pion π_s of momentum above 200 MeV/c with any $\mathrm{K}\pi$ or $\mathrm{K}\pi\pi\pi$ track combination. The track combinations for which the mass difference $m(\mathrm{K}\pi\pi_\mathrm{s}) - \mathrm{m}(\mathrm{K}\pi)$ or $m(\mathrm{K}\pi\pi\pi\pi_\mathrm{s}) - \mathrm{m}(\mathrm{K}\pi\pi\pi)$ is within ± 3.5 MeV/c^2 of the $m(\mathrm{D}^{*\pm}) - m(\mathrm{D}^0)$ mass difference are called $\mathrm{D}^{*\pm}$ candidates, while the remaining track combinations are called D^0 candidates. The $\mathrm{D}^{*\pm}$ candidates are excluded from the D^0 sample, which also includes B decays to D^{*0}, since the latter are not explicitly identified. With these criteria, less than 10% of the total number of $\mathrm{D}^{*\pm} \to \mathrm{D}^0\ \pi_s^\pm$ decays are incorrectly assigned to the D^0 sample.

To reduce the combinatorial background and improve the D mass resolution, the secondary vertices from B and D decays are reconstructed for all D decay channels except $\mathrm{D}^{*\pm} \to \mathrm{D}^0\ \pi^\pm(\mathrm{D}^0 \to \mathrm{K}\pi)$ [1]. The B mesons produced at $\sqrt{s} \simeq m_\mathrm{Z}$ have a typical decay length of 2.6 mm [19], which can be measured with an average resolution of 280 μm; this is used to differentiate tracks originating from the B or D decay point from those originating from the primary vertex. At least one VDET hit in both the $r\phi$ and z views is required for the lepton, the kaon and at least one π of momentum $p_\pi > 1$ GeV/c. A common D vertex is sought for the K and the pion(s) and a cut on the vertex χ^2 probability is applied. If a D vertex is identified, a common vertex for the lepton and the D candidate is searched for. This B vertex is required to lie between the event-by-event reconstructed interaction point and the D vertex. For the channels $\mathrm{B} \to \ell\nu_\ell \mathrm{D}^0\ X\ (\mathrm{D}^0 \to \mathrm{K}\pi\pi\pi)$ and $\mathrm{B} \to \ell\nu_\ell \mathrm{D}^\pm X\ (\mathrm{D}^\pm \to \mathrm{K}\pi\pi)$, a further reduction of the background is obtained by requiring the D vertex to lie at least 1 mm away from the interaction point.

The D mass distributions for the different channels are shown in Fig. 1. The resolution on the reconstructed D mass (see Table 1) is determined by fitting the $\mathrm{K}\pi$, $\mathrm{K}\pi\pi$ or $\mathrm{K}\pi\pi\pi$

[1] The statistics used for that channel is 1.66 million Z hadronic decays; it includes data taken before the installation of the ALEPH vertex detector.

Channel	Resolution (MeV/c^2)	D window (GeV/c^2)	Events Dℓ	Combinatorial Background
$D^0 \to K\pi$:				
B$\to \ell\nu_\ell D^{*\pm}(X)$	12	1.830-1.900	279 ± 20	47 ± 8
B$\to \ell\nu_\ell D^0\ (X)$	9	1.840-1.890	341 ± 21	43 ± 7
$D^0 \to K\pi\pi\pi$:				
B$\to \ell\nu_\ell D^{*\pm}(X)$	7	1.840-1.890	200 ± 18	57 ± 8
B$\to \ell\nu_\ell D^0\ (X)$	7	1.840-1.890	297 ± 21	237 ± 17
$D^\pm \to K\pi\pi$:				
B$\to \ell\nu_\ell D^\pm(X)$	7	1.845-1.895	278 ± 29	122 ± 13

Table 1. Resolution on the reconstructed D masses, mass windows used for counting events, estimated number of D mesons and combinatorial background in each channel. Errors indicated are statistical only.

mass distributions to a Gaussian superimposed on a linear background. The combinatorial background is estimated from two symmetric sidebands about the D mass peak, $1.73 < m_{\rm D} < 1.82$ and $1.91 < m_{\rm D} < 2$ GeV/c^2 for D^0 , $1.74 < m_{\rm D} < 1.83$ and $1.91 < m_{\rm D} < 2$ GeV/c^2 for $D^\pm$. The number of events counted inside the left and right sidebands are averaged and the number of background events is computed by scaling the resulting average to the width of the D mass windows. The number of D mesons is estimated by counting the events inside the mass windows defined in Table 1, after subtracting the combinatorial background. The estimated number of D mesons and of background combinations inside the D mass window are also given in Table 1. Summing over all decay channels, 1395 ± 50 D decays are reconstructed. The B$\to \ell\nu_\ell$D(X) selection efficiencies are determined by Monte Carlo using a Peterson et al. fragmentation function ($\langle x_E^{(\rm b)} \rangle = 0.693$). They range from about 8% to 25%, depending on the D decay channels.

4 B energy reconstruction

4.1 Method

To accurately measure the x_E spectrum, the B meson energy is estimated by summing the lepton, neutrino and D energies:

$$x_E^{(\rm B)} = \frac{E_l + E_{\rm D} + E_\nu}{E_{beam}}. \tag{5}$$

While the measurement of the lepton and D energies is straightforward, the neutrino energy E_ν must be estimated using a missing energy technique. The total visible energy E_{vis} in the lepton hemisphere is computed using the energy-flow algorithm described in Ref. [13]. Since in

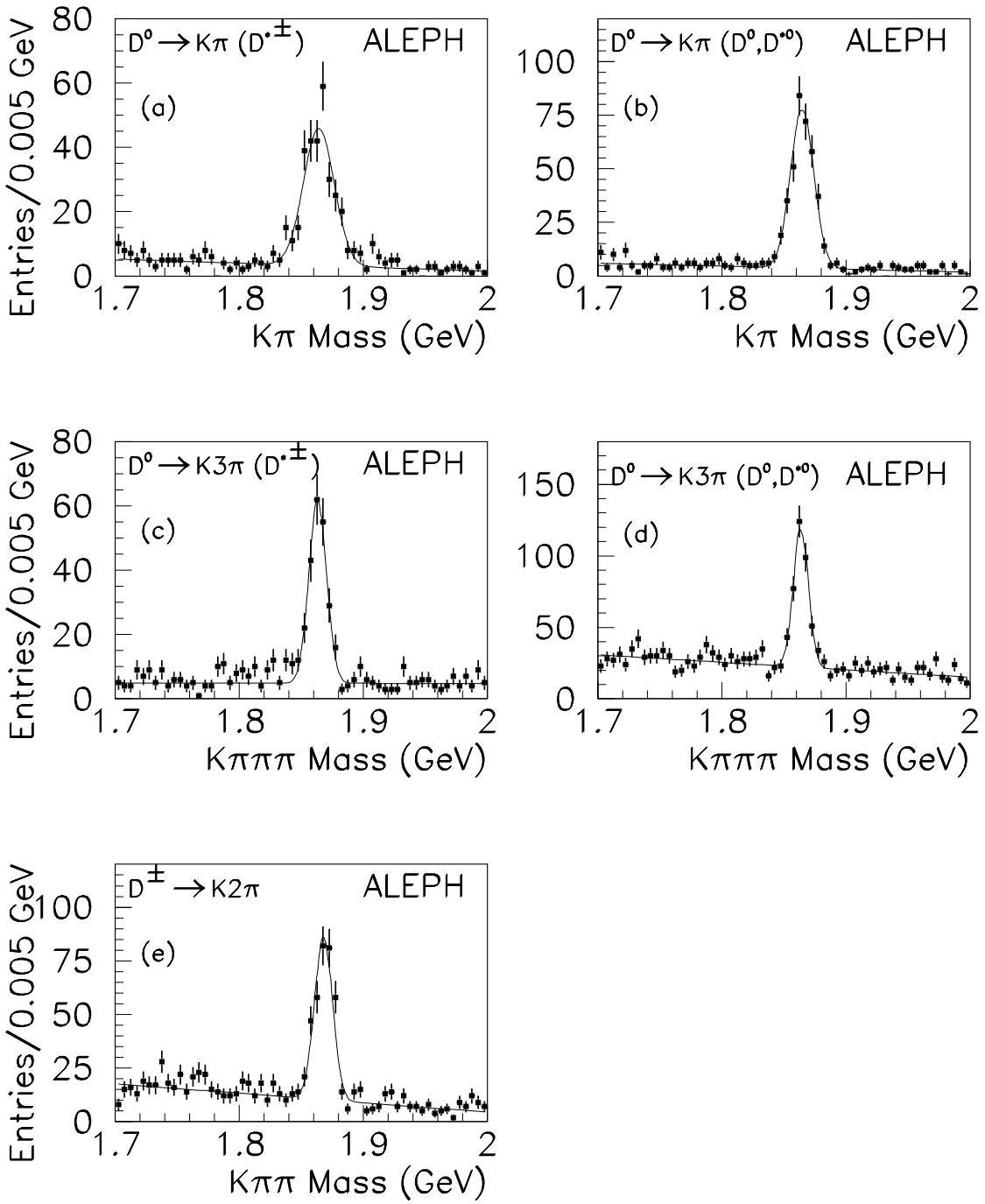


Figure 1: Reconstructed D mass spectra for the different decay channels:
(a) $B \to \ell\nu_\ell D^{*\pm}(D^{*\pm} \to D^0\pi^\pm,\ D^0 \to K\pi)$, ($b$) $B \to \ell\nu_\ell D^{0(*)}(D^0 \to K\pi)$,
(c) $B \to \ell\nu_\ell D^{*\pm}$ $(D^{*\pm} \to D^0\pi^\pm,\ D^0 \to K\pi\pi\pi)$, ($d$) $B \to \ell\nu_\ell D^{0(*)}(D^0 \to K\pi\pi\pi)$,
(e) $B \to \ell\nu_\ell D^\pm(D^\pm \to K\pi\pi)$.

the selected decay modes of the D neither neutrons nor K^0_L are expected, the neutral hadronic energy associated to the charged particles from the D is likely to be fake and is therefore not counted in E_{vis}. The reconstructed neutrino energy is then given by

$$E_\nu = E_{tot} - E_{vis}, \tag{6}$$

where E_{tot} is the total energy in the lepton hemisphere. From energy-momentum conservation

$$E_{tot} = E_{beam} + \frac{m^2_{same} - m^2_{opp}}{4E_{beam}}, \tag{7}$$

where m_{same}, m_{opp} are the hemisphere masses on lepton and opposite side respectively. They are computed using the four momenta of all particles in the appropriate hemisphere. Although m_{same} cannot be exactly computed due to the presence of a neutrino, Eq. (7) gives a more accurate estimate of the neutrino energy than approximating E_{tot} by E_{beam}, because the error on the hemisphere masses is small compared to the error on E_{vis} [20]. A mean resolution of approximately 2.4 GeV is obtained with this technique. The resolution depends on $x_E^{(\mathrm{B})}$ and improves from about 3.3 GeV for $x_E^{(\mathrm{B})} < 0.5$ to 1.8 GeV for $x_E^{(\mathrm{B})} > 0.9$.

4.2 Resolution and corrections

The difference between the reconstructed $x_E^{(\mathrm{B})}$ and the generated $x_E^{(\mathrm{b})}$ was studied using simulated data. The standard ALEPH Monte Carlo, HVFL03 [5], which is based on JETSET 7.3 [22], was used. More than 10000 events with full detector simulation were generated for each D decay mode studied. These events were also used to compute the acceptance and the detector resolution effects in the study of the b fragmentation described in Section 5.

The scaled energy measurement is mainly affected by the yet poorly known production (i) of excited D mesons and (ii) of excited B mesons.

(i) When a B decays to D^{*0} or D^{**}, the photons or pions emitted from the D^* or D^{**} decay are not explicitly identified, in this analysis, as a B decay product. The distributions of the difference between the reconstructed $x_E^{(\mathrm{B})}$ and the generated $x_E^{(\mathrm{b})}$ values are displayed in Fig. 2 for fully reconstructed decays $\mathrm{B}\rightarrow \ell\nu_\ell \mathrm{D}^0$, $\mathrm{D}^{*\pm}$ and for partially reconstructed decays $\mathrm{B}\rightarrow \ell\nu_\ell \mathrm{D}^{*0}$ or $\mathrm{B}\rightarrow \ell\nu_\ell \mathrm{D}^{**}$ with $\mathrm{D}^{**} \rightarrow \mathrm{D}^{*\pm}\pi$ and $\mathrm{D}^{**} \rightarrow \mathrm{D}^{(*)0}\pi$. Here, the primary b-hadron was either a B or a B^*. While the mean scaled energy is correctly estimated for fully reconstructed decays, it is underestimated by about 3% for decays to a D^{*0}, and by about 10% for decays to a D^{**}. For three-body decays $\mathrm{B}^0, \mathrm{B}^\pm \rightarrow \ell\nu_\ell \mathrm{D}^{(*)}$, the width of the resolution curve is dominated by the resolution of the reconstructed neutrino energy; for decays involving a D^{**}, the resolution is about 30% worse due to unidentified B decay products. An underestimation of $x_E^{(\mathrm{b})}$ in decays involving a D^{**} implies that the uncertainty on the fraction $f_{\mathrm{D}^{**}}$ of the semileptonic decays of the B into D^{**} directly affects the precision of the fragmentation measurement. This uncertainty is the main source of systematics in this analysis. From a compilation of recently published data [23, 24, 25, 26], a value $f_{\mathrm{D}^{**}} = 30 \pm 10\%$ was used in the analysis. An equal

proportion of resonant states and non-resonant decays $B \to \ell\nu_\ell D^{(*)}\pi$ was assumed, and $f_{D^{**}}$ was assumed to be the same in decays leading to a D^0, $D^\pm$ or $D^{*\pm}$ in the final state. The ratio $BR(B \to \ell\nu_\ell D^*)/BR(B \to \ell\nu_\ell D)$ was assumed to be 3, as expected from spin counting arguments.
(*ii*) When a b hadronizes to an excited B^* or B^{**} meson, photons or pions emitted from the excited B decay are not explicitly identified and $x_E^{(b)}$ is again underestimated. The B^*/B production ratio was recently measured [29, 30] and has a value compatible with three, as expected from spin counting arguments. This value is used in the Monte Carlo. Since the mean photon energy in $B^* \to B\gamma$ decays is low, the dependence of the $x_E^{(b)}$ measurement on the B^*/B production rate is negligible. On the other hand, the production of orbitally excited B states, as reported recently by LEP experiments [29, 31, 32], can affect significantly the b fragmentation measurement. Since B^{**} production is not described in HVFL03, the effect of such states was taken into account using a toy Monte Carlo model. It was assumed that the fragmentation function for $b \to B^{**}$ is the same as the fragmentation function for $b \to B, B^*$. A single spin 0 state B^{**} decaying to $B\pi$, with a mass difference $M(B\pi) - M(B) = 425$ MeV/c^2 [29], was produced with an energy distribution which was chosen according to the predictions of the fragmentation models considered. The x_E spectrum of the B mesons from B^{**} decays was built and the x_E spectra of the $B^{(*)}$ mesons for various proportions of $b \to B^{**}$ and various fragmentation models were then computed. In decays $B^{**} \to B\pi$, the pion carries about 7% of the primary b energy. Therefore, the fraction $f_{B^{**}} = N(b \to B^{**})/N(b \to B, B^*, B^{**})$ of B^{**} states in $\ell\nu_\ell D(X)$ events must be known to reconstruct the scaled energy distribution of the leading b-hadron produced by the b-quark. The value measured by ALEPH, $f_{B^{**}} = 27.9 \pm 7.2\%$ [29], was used in the analysis.

5 Study of b fragmentation

The raw $x_E^{(B)}$ distribution for the signal was reconstructed in nine bins between 0 and 1. For each bin, the signal was estimated by counting the number of events in the D^0 or $D^\pm$ mass peak, as described in Section 3. The raw spectra obtained for the various decay channels after subtraction of the predicted background from fake leptons correlated to a D meson (about 2% of the events) and from B decays to $D_s\bar{D}$, with D_s decaying semi-leptonically (about 1% of the events) are shown in Fig. 3. The analysis of the b fragmentation was then performed using two different methods:

- a comparison of the raw $x_E^{(B)}$ distributions with the predictions of existing fragmentation models;
- a model independent reconstruction of the shape of the $x_E^{(b)}$ spectrum, correcting the data points for acceptance, detector resolution and missed particles from B decays.

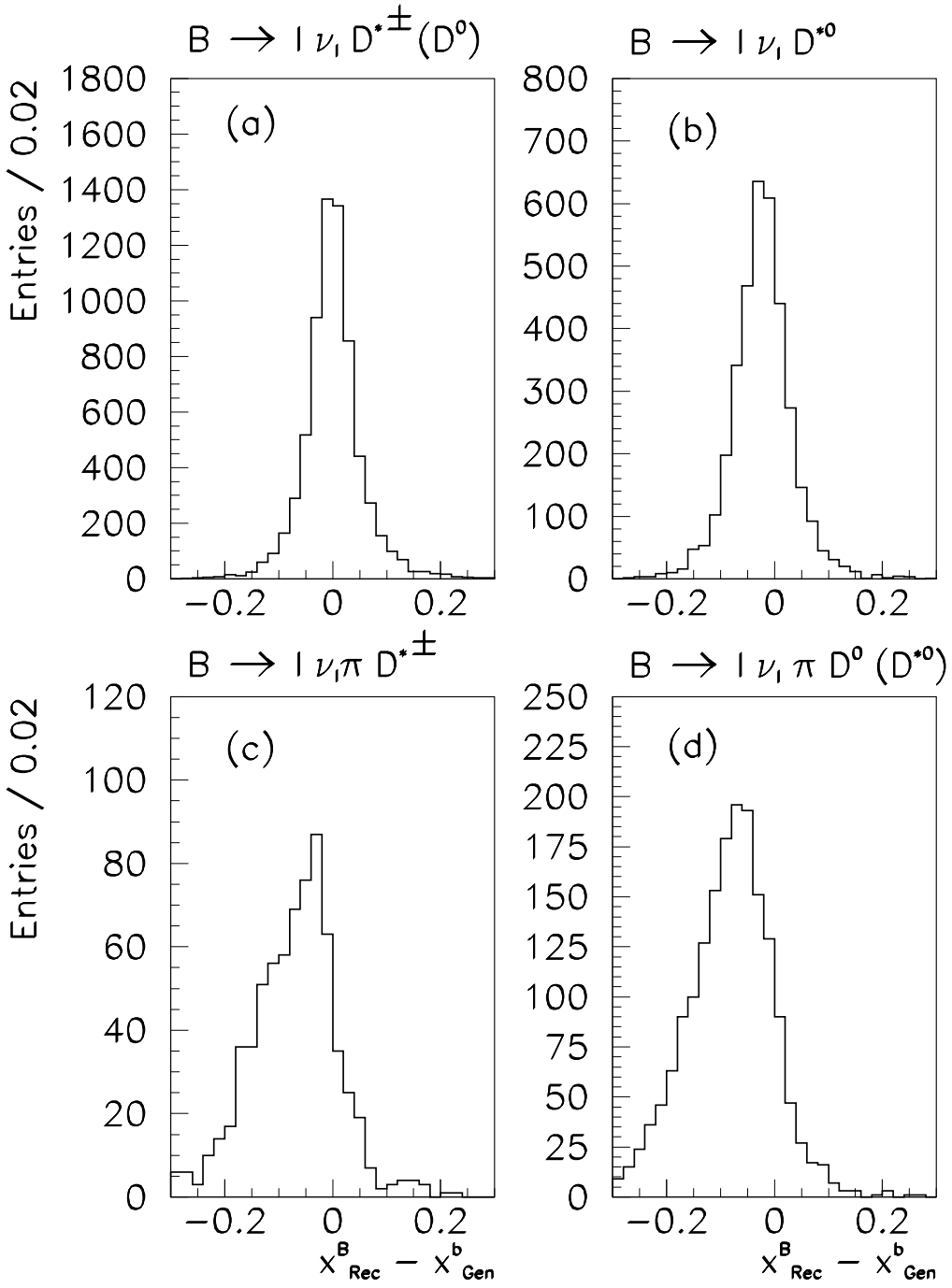


Figure 2: Difference between reconstructed $x_E^{(\mathrm{B})}$ and generated $x_E^{(\mathrm{b})}$ for the D decay channel $\mathrm{D}^0 \to \mathrm{K}\pi$: (a) fully reconstructed decays $\mathrm{B} \to \ell\nu_\ell \mathrm{D}^0$ and $\mathrm{B} \to \ell\nu_\ell \mathrm{D}^{*\pm}$ (b) partially reconstructed decays $\mathrm{B} \to \ell\nu_\ell \mathrm{D}^{*0}$, (c) $\mathrm{B} \to \ell\nu_\ell \mathrm{D}^{*\pm}\pi$ and (d) $\mathrm{B} \to \ell\nu_\ell \mathrm{D}^{(*)0}\pi$. The distributions obtained for the other D meson decay channels are similar.

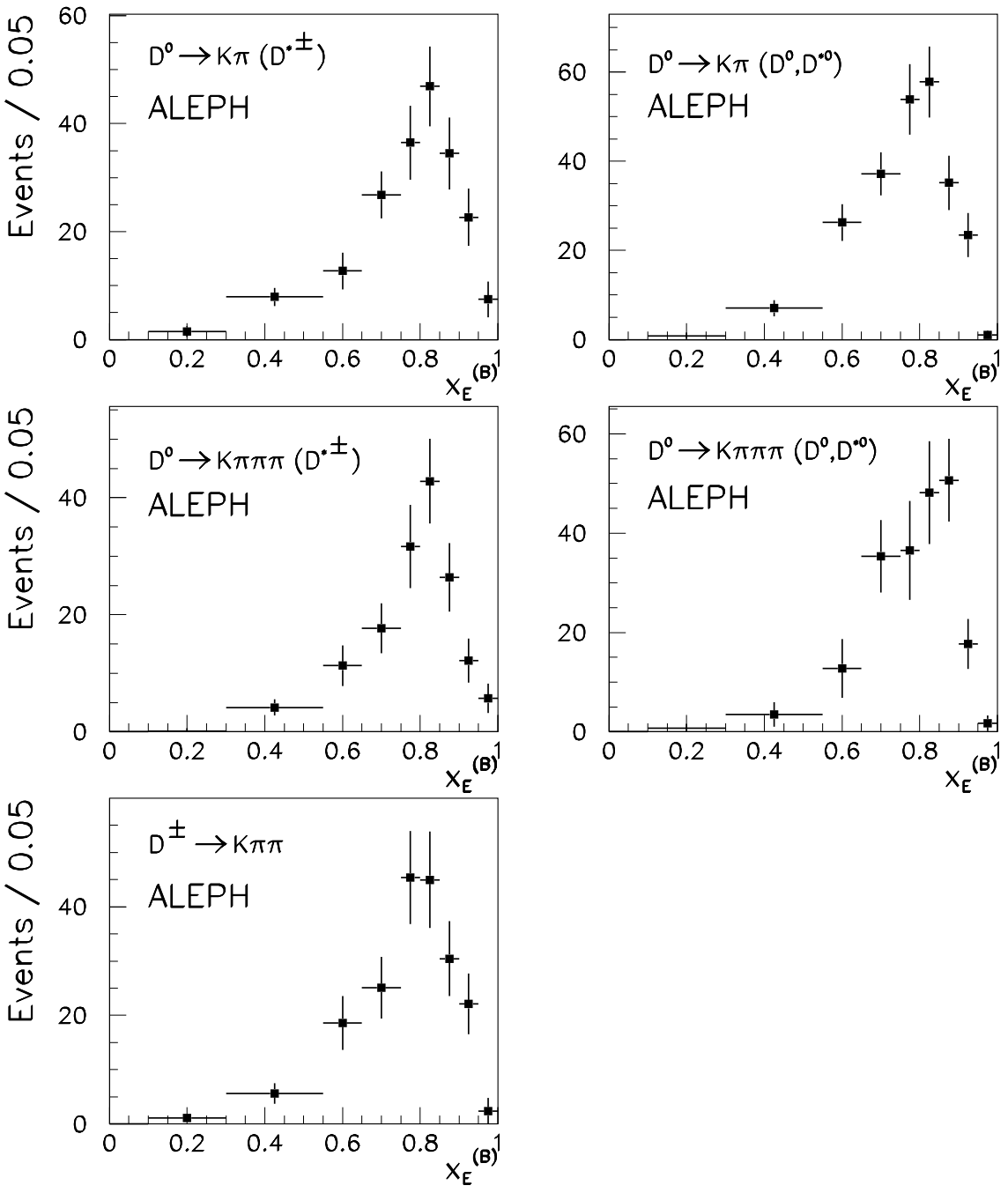


Figure 3: Reconstructed $x_E^{(\mathrm{B})}$ distributions for the different decay channels before efficiency corrections.

Channel	Weight	$\langle x_E^{(b)} \rangle$
$D^0 \to K\pi$:		
$B \to \ell\nu_\ell D^{*\pm}(X)$	28%	0.706 ± 0.012
$B \to \ell\nu_\ell D^0(X)$	33.3%	0.719 ± 0.012
$D^0 \to K\pi\pi\pi$:		
$B \to \ell\nu_\ell D^{*\pm}(X)$	14.8%	0.714 ± 0.017
$B \to \ell\nu_\ell D^0(X)$	9.0%	0.738 ± 0.025
$D^\pm \to K\pi\pi$:		
$B \to \ell\nu_\ell D^\pm(X)$	14.9%	0.706 ± 0.018
combined		0.715 ± 0.007

Table 2: The statistical weight of each channel and the mean $x_E^{(b)}$ of b-hadrons found for that channel. The mean $x_E^{(b)}$ is computed using the corrected data points for each channel, assuming $f_{D^{**}}$=30% and $f_{B^{**}}$=27.9%. Errors indicated are statistical only.

5.1 Comparison to fragmentation models

The measured $x_E^{(B)}$ distribution is compared to the prediction of different fragmentation models used in JETSET 7.3 [22] parton shower Monte Carlo with string fragmentation [21]. In this model, the fragmentation parameters are correlated with the QCD scale parameter Λ_{JETSET}, and with the shower cutoff mass M_{min}. From a comparison of the JETSET Monte Carlo to the ALEPH data [27], the values $\Lambda_{JETSET} = 311$ MeV and $M_{min} = 1.9$ GeV were determined. The following parametrizations of the fragmentation function were tried:

$$\text{Peterson et al. [1]} \qquad D_b^H(z) \propto \frac{1}{z}\left(1 - \frac{1}{z} - \frac{\epsilon_b}{1-z}\right)^{-2} \tag{8}$$

$$\text{Kartvelishvili et al. [2]} \qquad D_b^H(z) \propto z^{\alpha_b}(1-z) \tag{9}$$

$$\text{Collins and Spiller [3]} \qquad D_b^H(z) \propto \left(\frac{1-z}{z} + \frac{(2-z)\epsilon_b}{1-z}\right)\left(1+z^2\right)\left(1 - \frac{1}{z} - \frac{\epsilon_b}{1-z}\right)^{-2} \tag{10}$$

$$\text{Lund symmetric [4]} \qquad D_b^H(z) \propto \frac{1}{z}(1-z)^a exp(-0.5m_T^2/z) \tag{11}$$

The JETSET 7.3 Monte Carlo was used to convert these distributions into $x_E^{(b)}$ spectra. The data were also compared to the predictions of the cluster fragmentation model used in the HERWIG Monte Carlo [28], tuned to reproduce ALEPH data [27].

Monte Carlo events $B \to \ell\nu_\ell D^{(*)}X$ with full detector simulation were passed through the same analysis chain as the data and the reconstructed $x_E^{(B)}$ distribution of the real events was compared to that of the selected Monte Carlo events. A simulation of the different fragmentation functions was obtained from reweighting events according to the z distributions predicted for the various models. To reach the best statistical sensitivity, the five decay channels used

in the analysis were combined together. Because of the different backgrounds, the statistical weights ω_{ch} of each decay channel were computed separately and are given in Table 2. The bin $x_E^{(\mathrm{B})} < 0.3$, for which the acceptance is close to zero in all decay channels, was not used in the analysis. To combine the five spectra, the normalized $x_E^{(\mathrm{B})}$ spectra for each channel were constructed, both for the data and for the Monte Carlo, and summed together with the relative weights ω_{ch}. If $N_k^{obs}(ch)$ is the number of events observed in bin k for channel ch, the fraction of events in bin k for the combined distribution is:

$$\rho_k^{(obs)} = \sum_{ch} \omega_{ch} \cdot \frac{N_k^{obs}(ch)}{\sum_{i=2}^{i=9} N_i^{obs}(ch)}. \tag{12}$$

The best fit to each model is obtained by minimizing

$$\chi^2 = \sum_{k=2}^{k=9} \frac{\left(\rho_k^{(obs)}(data) - \rho_k^{(obs)}(MC)\right)^2}{\sigma_k^2}, \tag{13}$$

where σ_k takes into account the statistical uncertainty in both data and Monte Carlo. The fitted parameter values are listed in Table 3, together with the corresponding mean energy fraction of the B mesons and the χ^2 probabilities. Errors indicated are statistical only. The systematic uncertainties are discussed in Section 6. Because the uncertainty on $f_{\mathrm{D}^{**}}$ is the main source of systematic error, the results are given both for $f_{\mathrm{D}^{**}}$=30% and for the upper and lower allowed values $f_{\mathrm{D}^{**}}$=40 and 20%. The χ^2 probabilities given in Table 3 show that the Peterson, Kartvelishvili and Lund symmetric fragmentation functions are favoured by the data, while the Collins and Spiller model gives a poor fit. As mentioned in [27], the mean scaled energy of b-hadrons produced in HERWIG is lower than in the data. This is clearly illustrated in Fig. 4, which shows the combined $x_E^{(\mathrm{B})}$ spectra for the data compared to the HERWIG prediction; the predictions of the other fragmentation models, with parameters adjusted to give the best fit to the data, are also shown in the same figure.

The above conclusions are not affected if B^{**} production is ignored. In that case, the best fits correspond to a decrease of 0.015 of the mean scaled energy.

5.2 Model-independent analysis

In this section the reconstructed $x_E^{(\mathrm{B})}$ spectra for each channel are corrected for acceptance, detector resolution and missing particles (π, γ) and are combined together. This provides a nearly model-independent estimate of the shape of the fragmentation function.

For a given channel, the true number of events in bin i, $N_i^{true}(ch)$, can be unfolded from

$$N_i^{true}(ch) = \frac{\sum_k G_{ik}(ch) N_k^{obs}(ch)}{\epsilon_i(ch)}, \tag{14}$$

where $N_k^{obs}(ch)$ is the observed number of events in bin k for the channel ch, $G_{ik}(ch)$ is the resolution matrix, *i.e.* the fraction of events with true $x_E^{(\mathrm{b})}$ in bin i reconstructed in bin k, and

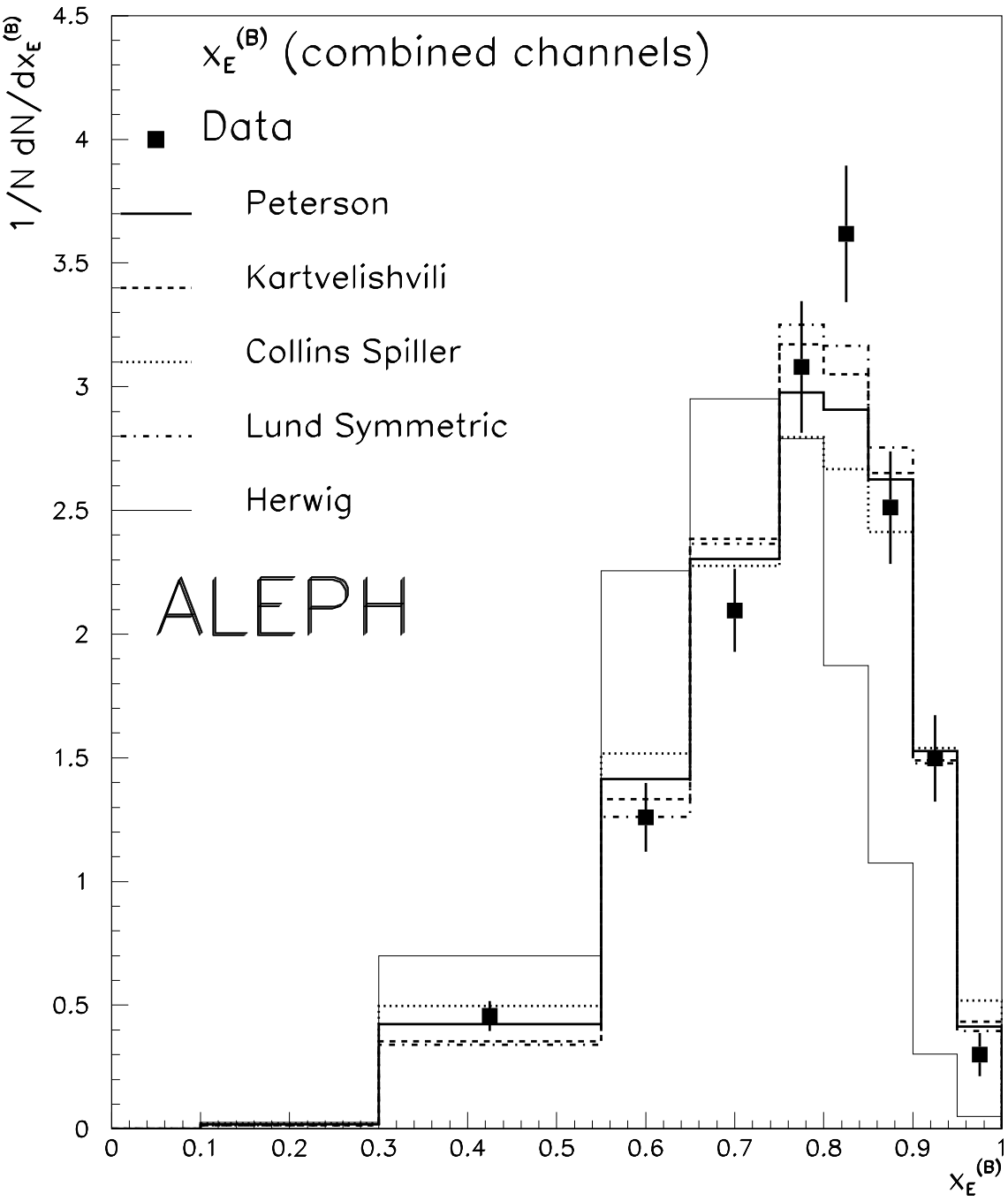


Figure 4: The measured scaled energy distribution of the reconstructed B mesons (before efficiency correction) combining all modes, compared to the predictions of different fragmentation models, for $f_{\mathrm{D}^{**}} = 30\%$. The fragmentation parameters correspond to the best fit to the data; they are given in Table 3.

Model	$f_{\mathrm{D}^{**}}$	Parameter	$\langle x_E^{(\mathrm{b})} \rangle$	χ^2/NDF	Probability
Peterson	0.20	$\epsilon_b = 0.0038 \pm 0.0006$	0.708 ± 0.0006	9.1 / 7	24%
et al.	0.30	$\epsilon_b = 0.0030 \pm 0.0005$	0.716 ± 0.0006	10.5 / 7	18%
	0.40	$\epsilon_b = 0.0024 \pm 0.0005$	0.722 ± 0.0006	12.1 / 7	10%
Kartvelishvili	0.20	$\alpha_b = 13.3 \pm 1.0$	0.726 ± 0.0006	11.6 / 7	12%
et al.	0.30	$\alpha_b = 14.7 \pm 1.1$	0.732 ± 0.0006	11.7 / 7	12%
	0.40	$\alpha_b = 16.5 \pm 1.2$	0.739 ± 0.0006	11.9 / 7	11%
Collins &	0.20	$\epsilon_b = 0.0022 \pm 0.0006$	0.692 ± 0.0004	18.6 / 7	1%
Spiller	0.30	$\epsilon_b = 0.0016 \pm 0.0005$	0.697 ± 0.0006	21.2 / 7	<0.5%
	0.40	$\epsilon_b = 0.0010 \pm 0.0004$	0.705 ± 0.0006	23.9 / 7	<0.5%
Lund	0.20	$a = 1.30 \pm 0.15$	0.729 ± 0.004	11.3 / 7	13%
Symmetric	0.30	$a = 1.10 \pm 0.15$	0.735 ± 0.004	10.4 / 7	18%
	0.40	$a = 0.95 \pm 0.15$	0.740 ± 0.004	10.7 / 7	17%
Herwig	0.30	none	0.627	230 / 7	<0.1%

Table 3: Minimal χ^2 and corresponding values of the fragmentation function parameter for the fit of the measured $x_E^{(\mathrm{b})}$ spectra with different fragmentation models. Errors quoted are statistical only. These results were obtained assuming $f_{\mathrm{B}^{**}} = 27.9\%$

$\epsilon_i(ch)$ is the mean acceptance for bin i. Because the matrix elements G_{ik} depend on the B energy distribution, Eq. (14) has to be solved iteratively. The main technical points are: (i) choosing a first estimate of $G_{ik}^{(0)}$; (ii) combining the five different decay channels; and (iii) describing, at each iteration, the B meson energy distribution in the Monte Carlo with a function $f_n(x_E^{(\mathrm{b})})$.
(i) Initially, the reciprocal of the resolution function for each channel is approximated by the unity matrix, $G_{ik}^{(0)}(ch) = \delta_{ik}$. This approximation gives a first estimate $N_i^{true\ (1)}(ch) = N_i^{obs}(ch)/\epsilon_i(ch)$ of the acceptance corrected number of events in the bin i. Since the acceptance of the bin $x_E^{(\mathrm{b})} < 0.3$ is close to 0, the number of events N_1^{true} in that bin must be extrapolated from the content of the other bins. At the first iteration, N_1^{true} is assumed to be 4.3% of the total events, which is the prediction using Eq. (1) with $\langle x_E^{(\mathrm{b})} \rangle$=0.693. In subsequent iterations N_1^{true} is obtained by integrating over the bin the parametrization $f_n(x_E^{(\mathrm{b})})$ of the corrected $x_E^{(\mathrm{b})}$ spectrum resulting from the previous iteration.
(ii) Secondly, the normalized $x_E^{(\mathrm{b})}$ spectra for each decay channel are built and combined according to

$$\frac{1}{N} \cdot \left. \frac{dN}{dx_E^{(\mathrm{b})}} \right|_{bin\ k} = \sum_{ch} \omega_{ch} \cdot \frac{N_k^{true}(ch)}{\sum_i N_i^{true}(ch)}. \tag{15}$$

The statistical weights ω_{ch} of each decay channel are computed as mentioned in the previous Section.
(iii) Finally, to ensure the convergence of the iterative procedure, and to avoid spurious peaks

arising from statistical fluctuations inherent to any iterative method, the fragmentation is constrained to be described by a smooth curve with a single maximum. A three parameters shape

$$f(x_E^{(\mathrm{b})}) = K \frac{1 + a(1 - x_E^{(\mathrm{b})})}{x_E^{(\mathrm{b})}} \cdot \left(1 - \frac{b}{x_E^{(\mathrm{b})}} - \frac{c}{1 - x_E^{(\mathrm{b})}}\right)^{-2} \tag{16}$$

is found to be the best parametrization of the data. The fitted curve is introduced in the Monte Carlo to describe the energy distribution of simulated B mesons and the resolution matrix G_{ik} is reestimated. Eq. (16) is only an *ad hoc* parametrization used to smooth the data spectrum in the iterative correction.

The procedure described above is iterated until each point moves by less than 10% of its statistical error. With this criterion, the convergence is reached after seven iterations.

This procedure has been tested by generating Monte Carlo "toy experiments" with different fragmentation functions. The convergence to the generated distribution always occurs in less than ten iterations. Many different shapes are statistically compatible with the data (see Section 5.1). While the final result is computed using the best parametrization found, the model dependence of the results is studied by testing other allowed parametrizations. This is discussed in the following section. Stability of the final result against the initial conditions (values $G_{ik}(0)$ assumed when starting the iterations) and against the convergence criterion was also checked and no dependence was found.

6 Systematics and final result

Systematics due to physics, to detector and to model dependence of the correction procedure were considered. The main systematic error due to physics is the poor knowledge of the branching fractions of the B into $\ell\nu_\ell \mathrm{D}^{**}$, $\mathrm{D}\pi$ and $\mathrm{D}^*\pi$. Uncertainties on the D^*/D ratio and on the background subtraction were also considered, as well as those arising from B^{**} production in the b-quark hadronization. Detector effects are reflected by a systematic uncertainty in the neutrino energy measurement. The model dependent systematic error incorporates the uncertainty on the estimate of the number of events at $x_E^{(\mathrm{b})} < 0.3$, which is related to the dependence of the final result on the choice of the parametrization curve $f(x_E^{(\mathrm{b})})$.

The size of the different systematics effects was quantified by looking at the variation of mean $x_E^{(\mathrm{b})}$, computed from the data points only with

$$\langle x_E^{(\mathrm{b})} \rangle = \frac{1}{N} \sum_{k=1}^{k=9} N_k \cdot \langle x_E \rangle_k, \tag{17}$$

where N_k is the number of events in bin k and $\langle x_E \rangle_k$ is defined as

$$\langle x_E \rangle_k = \frac{\int x f(x) \mathrm{dx}}{\int \mathrm{f(x)dx}}, \tag{18}$$

the integration being performed over the bin k. The various contributions to the systematics are the following.

- D^{**} fraction in B semileptonic decays: the systematic error due to the uncertainty on $f_{D^{**}}$ was estimated by repeating the analysis for a variation $\Delta f_{D^{**}} = \pm 0.1$, as expected from a study of recent experimental results [23, 24, 25, 26]. The systematic error on the mean $x_E^{(b)}$ is $\Delta\langle x_E^{(b)}\rangle = \pm 0.010$

- D^{**} model: while there is clear experimental evidence for the decay $B \to \ell^{\pm}\nu_\ell D_{2420}^{**}$ [23, 25, 26], other unidentified semileptonic B decays could either include heavier resonant states D_J^{**}[26] or non-resonant decays $B \to \ell^{\pm}\nu_\ell D^{(*)}\pi$[25]. For the latter, the energy carried by the missing π is expected to be about 10% higher than in resonant decays. The corresponding uncertainty on $x_E^{(b)}$ is $\Delta\langle x_E^{(b)}\rangle = \pm 0.002$

- D^*/D ratio: this ratio can affect the result by changing the fraction of $B \to \ell\nu_\ell D^{*0}$ decays in the sample of $B \to \ell\nu_\ell D^0$ (X) events. By changing this ratio from 3 to 2, a variation of the mean $x_E^{(b)}$ $\Delta\langle x_E^{(b)}\rangle = 0.001$ is obtained.

- B^{**} fraction in B semileptonic decays: from [29], the uncertainty on $f_{B^{**}}$ is estimated to ± 0.072. The corresponding uncertainty on the mean $x_E^{(b)}$ of the leading b-hadron produced in the b-quark hadronization is $\Delta\langle x_E^{(b)}\rangle = \pm 0.004$

- B^{**} model: the estimated uncertainty on the mean mass of B^{**} states produced is ± 20 MeV/c^2 [29]. The corresponding uncertainty on the mean $x_E^{(b)}$ is $\Delta\langle x_E^{(b)}\rangle = \pm 0.001$. Other modelling uncertainties (B^{**} width, angular distribution of decay products) have an even smaller effect.

- Background subtraction: this background comes from all processes (but primary semileptonic B decays) leading to a reconstructed lepton correlated to a D meson in the same hemisphere. From the uncertainty on the branching ratios $B \to D_s\bar{D}(X)$ and the statistical error on the Monte Carlo sample, a $\pm 70\%$ error on this background was assigned. The corresponding variation of $x_E^{(b)}$ is $\Delta\langle x_E^{(b)}\rangle = \pm 0.002$

- Neutrino energy reconstruction: the hemisphere energy reconstruction was checked by computing the neutrino energy in each hemisphere (according to Eq. 6 and 7) for an inclusive sample of events containing a high transverse momentum lepton with $p_T > 1$ GeV/c. It can be seen from Fig. 5 that the neutrino energy distribution for the data is rather well reproduced by the simulation, both for the lepton hemisphere, in which a neutrino is always expected, and for the opposite hemisphere: no significant shift is observed and the detector resolution is correctly simulated. The precision on the neutrino energy calibration is therefore estimated to be 100 MeV, from which a systematic uncertainty $\Delta\langle x_E^{(b)}\rangle = 0.002$ on $x_E^{(b)}$ results.

- Uncertainty on the number of events extrapolated in the bin $x_E^{(b)} < 0.3$ and choice of the parametrization curve $f(x_E^{(b)})$: since $f(x_E^{(b)})$ is used both for the correction and to

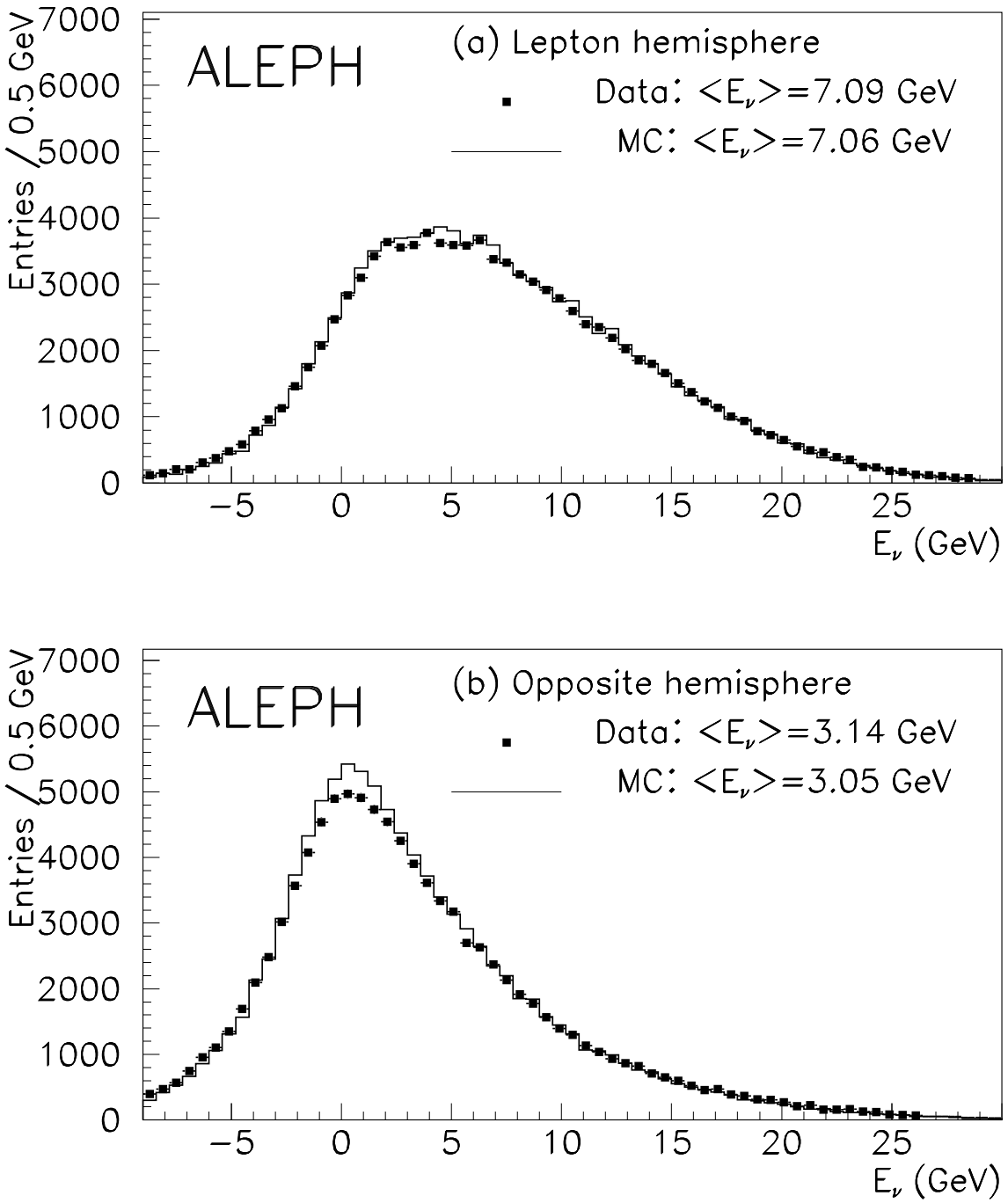


Figure 5: The neutrino energy reconstructed in (a) the lepton hemisphere and (b) in the opposite hemisphere for inclusive leptons with $p_T > 1$ GeV/c. Black squares are for data, histogram is for simulation.

Systematic	$\Delta\langle x_E^{(b)}\rangle$
$f_{D^{**}}$	± 0.010
D^{**} model	± 0.002
D^*/D ratio	± 0.001
$f_{B^{**}}$	± 0.004
B^{**} mass	± 0.001
Background	± 0.002
E_ν	± 0.002
$f(x_E^{(b)})$	± 0.006
combined	± 0.013

Table 4: Summary of the main systematic errors of $\langle x_E^{(b)}\rangle$.

estimate the number of events at $x_E^{(b)} < 0.3$, the two effects are treated as one systematic uncertainty. From the comparison with the fragmentation models in Section 5.1, it can be seen that the $x_E^{(b)}$ spectra predicted using the Peterson et al., Kartvelishvili et al. and Lund symmetric fragmentation models cover approximately the range of shapes compatible with the data. Therefore, a conservative estimate of the systematic error due to the uncertainty on the parametrization $f(x_E^{(b)})$ was obtained by repeating the analysis using the $x_E^{(b)}$ distributions of these fragmentation models instead of Eq. (16). The corresponding uncertainty on mean $x_E^{(b)}$ is $\Delta\langle x_E^{(b)}\rangle = \pm 0.006$ and is mostly due to the difference in the fraction of events at low $x_E^{(b)}$ between the different models.

The effects of the main systematic errors on the mean $x_E^{(b)}$ are summarized in Table 4. The dominant errors are the uncertainties on the D^{**} and B^{**} contributions and the model dependence of the correction. Combining all the systematics, the error on the mean $x_E^{(b)}$ is :

$$\Delta\langle x_E^{(b)}\rangle = \pm 0.013.$$

The $x_E^{(b)}$ spectrum of the leading b-meson produced is shown in Fig. 6. The contents of each bin, together with the statistical and the systematic error on that number, are given in Table 5. The systematic errors due to the uncertainty on the D^{**} and B^{**} contributions are given separately in the tables while, in the figures, they have been incorporated in the global systematic error. The influence of D^{**} states is illustrated in Fig. 6 by showing the best fits to the data points for $f_{D^{**}}$=20%, 30% and 40%. In Fig. 7, the same spectrum is compared to the predictions of the different fragmentation models, for the best fit values of the fragmentation parameters and a D^{**} contribution $f_{D^{**}}$=30%. In Table 6, the correlation matrix for the statistical errors, which is non-diagonal due to the bin-to-bin correlation introduced by the deconvolution method, can be found.

The mean energy fraction of the leading b-mesons is $\langle x_E^{(b)}\rangle = 0.715 \pm 0.007(\text{stat}) \pm 0.013(\text{syst})$. This value is in good agreement with analyses of inclusive lepton momentum spectra [5, 6, 7, 8].

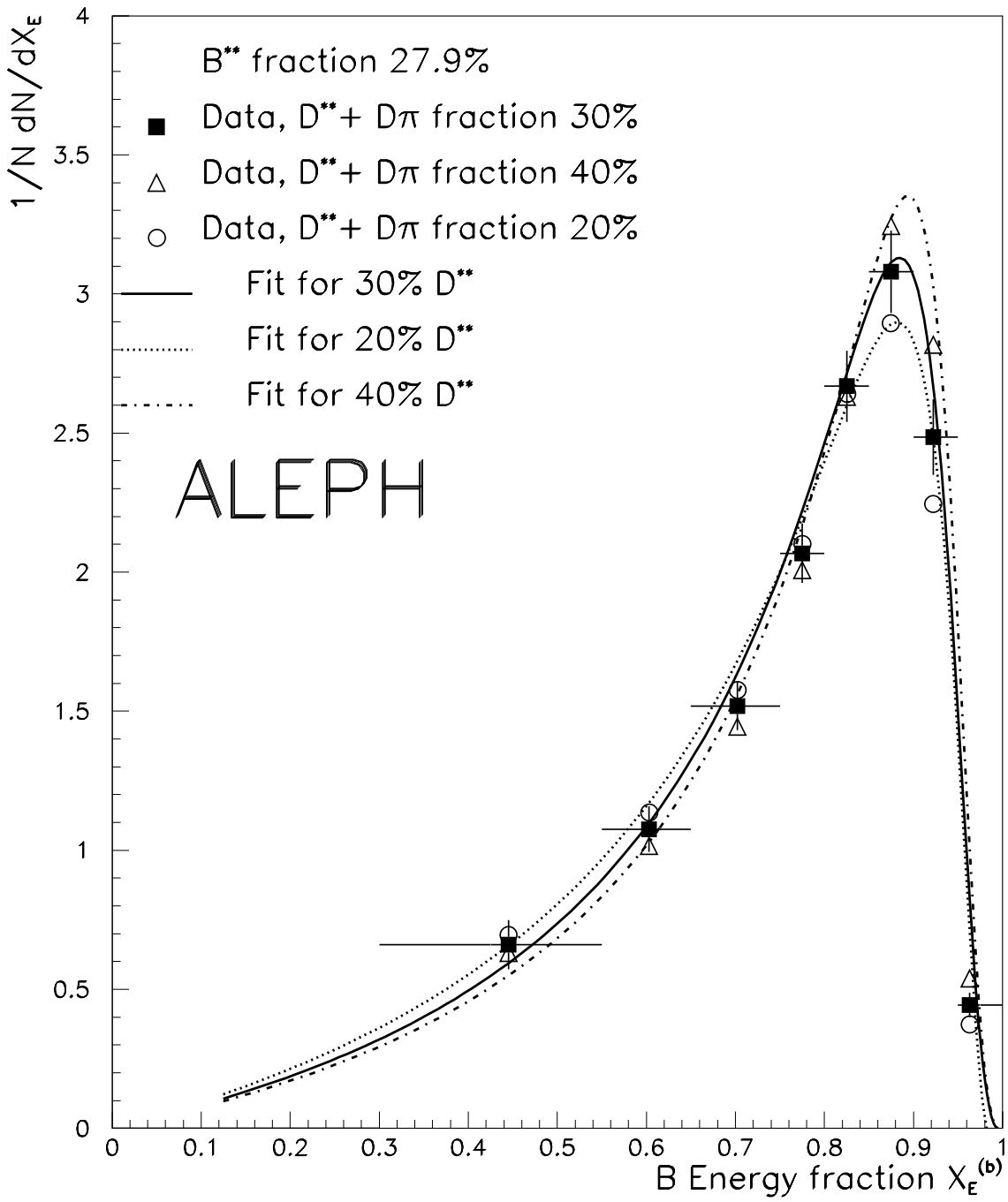


Figure 6: The acceptance corrected $x_E^{(\mathrm{b})}$ spectrum of the leading b-mesons combining all channels, for $f_{\mathrm{D}^{**}}$=20, 30 and 40%. The error shown is statistical only and does not account for the point-to-point correlations induced by the deconvolution process. It is only shown for $f_{\mathrm{D}^{**}}$=30%. Also shown are the fit results of Eq. 16 for $f_{\mathrm{D}^{**}}$=20, 30 and 40%.

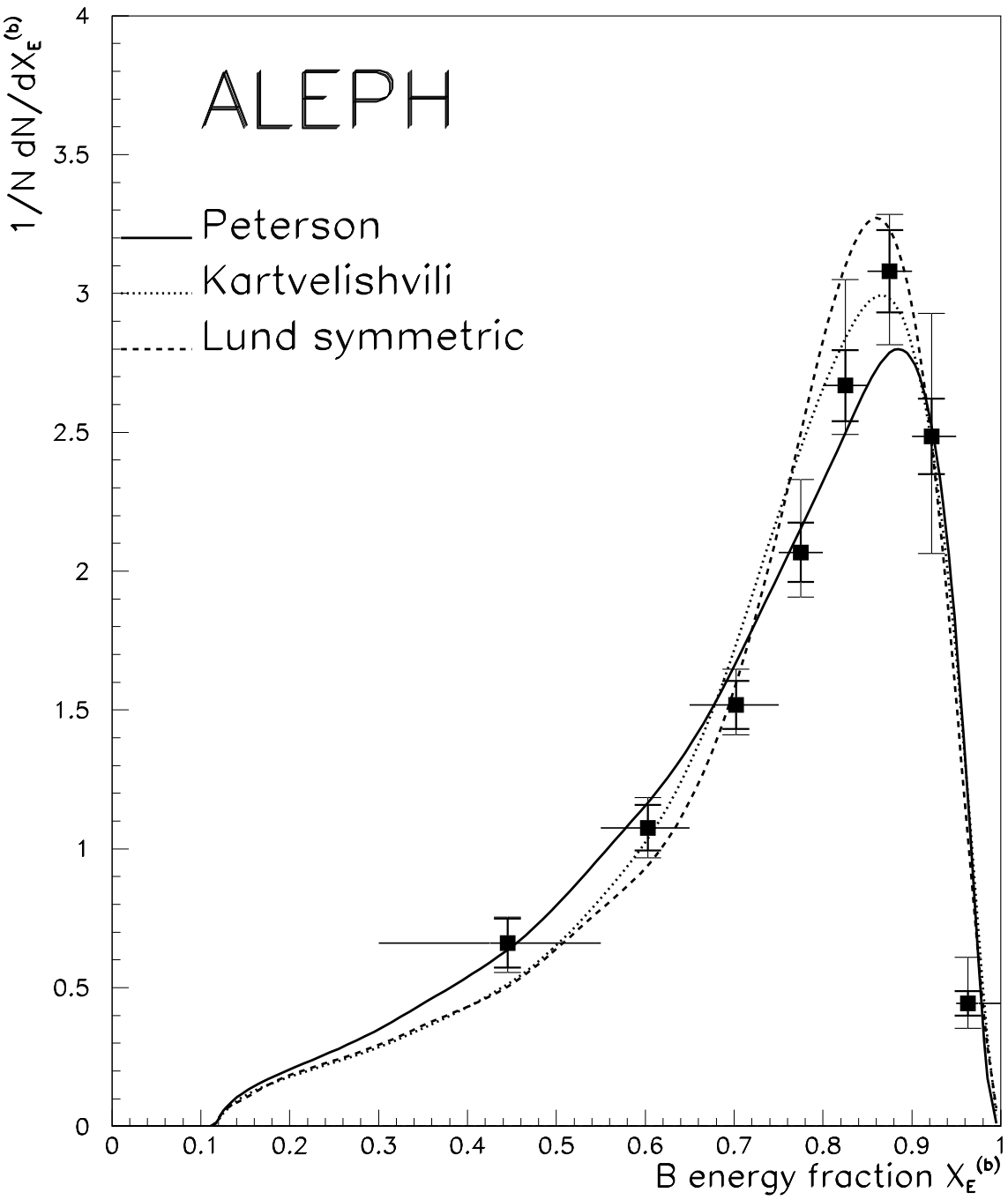


Figure 7: The acceptance corrected $x_E^{(\mathrm{b})}$ spectrum of the leading b-meson for $f_{\mathrm{B}^{**}}$=27.9% and $f_{\mathrm{D}^{**}}$=30%, compared with the predictions of different fragmentation models. The smaller error bar is statistical. The larger one is the sum of statistical + systematic errors. The errors shown do not account for the point-to-point correlations induced by the deconvolution process.

$x_E^{(b)}$ Bin Limits	Event Fraction
0.30-0.55	$0.165 \pm 0.019\ ^{+0.002}_{-0.012}\ ^{-0.007}_{+0.008}\ ^{-0.003}_{+0.002}$
0.55-0.65	$0.108 \pm 0.008\ ^{+0.003}_{-0.007}\ ^{-0.006}_{+0.008}\ ^{-0.001}_{+0.001}$
0.65-0.75	$0.152 \pm 0.009\ ^{+0.009}_{-0.001}\ ^{-0.008}_{+0.007}\ ^{-0.002}_{+0.004}$
0.75-0.80	$0.103 \pm 0.005\ ^{+0.011}_{-0.002}\ ^{-0.005}_{+0.002}\ ^{-0.004}_{+0.002}$
0.80-0.85	$0.133 \pm 0.006\ ^{+0.018}_{-0.004}\ ^{-0.004}_{+0.000}\ ^{-0.005}_{+0.001}$
0.85-0.90	$0.154 \pm 0.007\ ^{+0.003}_{-0.006}\ ^{+0.005}_{-0.009}\ ^{+0.002}_{-0.003}$
0.90-0.95	$0.124 \pm 0.007\ ^{+0.005}_{-0.013}\ ^{+0.020}_{-0.013}\ ^{+0.010}_{-0.008}$
0.95-1.	$0.022 \pm 0.002\ ^{+0.007}_{-0.001}\ ^{+0.004}_{-0.003}\ ^{+0.002}_{-0.003}$

Table 5: The measured $x_E^{(b)}$ spectrum (fraction of events in each bin) for the leading b-meson produced. The first error is statistical, the second one is systematic (excluding the uncertainty on D^{**} and B^{**} contributions) and the third and fourth ones are the systematics due to a variation $\Delta f_{D^{**}} = \pm 0.1$ and $\Delta f_{B^{**}} = \pm 0.072$.

$0.30 < x_E^{(b)} < 0.55$	1.000	0.625	0.226	0.081	0.051	0.024	0.018	0.006
$0.55 < x_E^{(b)} < 0.65$	-	1.000	0.618	0.287	0.180	0.092	0.055	0.020
$0.65 < x_E^{(b)} < 0.75$	-	-	1.000	0.676	0.454	0.257	0.140	0.059
$0.75 < x_E^{(b)} < 0.80$	-	-	-	1.000	0.672	0.476	0.256	0.107
$0.80 < x_E^{(b)} < 0.85$	-	-	-	-	1.000	0.673	0.438	0.183
$0.85 < x_E^{(b)} < 0.90$	-	-	-	-	-	1.000	0.621	0.317
$0.90 < x_E^{(b)} < 0.95$	-	-	-	-	-	-	1.000	0.518
$0.95 < x_E^{(b)} < 1.$	-	-	-	-	-	-	-	1.000

Table 6: The bin-to-bin statistical correlation matrix for $f_{D^{**}}$=30% and $f_{B^{**}}$=27.9%.

For the latter, B^{**} production was not accounted for and therefore the mean $x_E^{(b)}$ quoted are lower by 0.015. On the other hand this measurement does not include the effect of b baryon production, while the analyses of [5, 6, 7, 8] do. The mean $x_E^{(b)}$ is increased by 0.001 when b-baryon production is included.

7 Conclusion

Using about 1400 semileptonic B^0 and $B^{\pm}$ decays with reconstructed D mesons, the shape of the effective b fragmentation function has been measured directly. Assuming that the contribution of the D^{**} states to the semileptonic B decays is $f_{D^{**}} = 30 \pm 10\%$ and that the B^{**} states represent a fraction $f_{B^{**}} = 27.9 \pm 7.2\%$ of the b-mesons produced, the mean scaled energy of the leading b-meson produced in the b-quark hadronization is

$$\langle x_E^{(b)} \rangle = 0.715 \pm 0.007(\text{stat}) \pm 0.013(\text{syst})$$

which is consistent with previous measurements [5].

Furthermore, this analysis improves on [11] and gives the most precise direct measurement of the shape of the fragmentation function to date. The $x_E^{(b)}$ distribution observed (Fig. 7) has been compared with the predictions of different fragmentation models. The Peterson et al. [4], Kartvelishvili et al. [2] and Lund symmetric [4] models were found to be compatible with the observed $x_E^{(b)}$ spectrum, with corresponding χ^2 probabilities of 18%, 10% and 18% respectively, while the Collins and Spiller [3] fragmentation function is disfavoured by the data (χ^2 probability less than 0.5%). The scaled energy distribution of b-hadrons obtained with HERWIG does not agree with the data.

8 Acknowledgements

We wish to thank our colleagues from the accelerator divisions for the successful operation of LEP. We are indebted to the engineers and technicians in all our institutions for their contribution to the excellent performance of ALEPH. Those of us from non member countries thank CERN for its hospitality.

References

[1] C.Peterson, D.Schlatter, I.Schmitt, P.M.Zerwas, Phys. Rev. **D27** (1983) 105.

[2] V.G.Kartvelishvili, A.K. Likehoded, V.A.Petrov, Phys. Lett. **B78** (1978) 615.

[3] P.Collins and T.Spiller, J. Phys. **G11** (1985) 1289.

[4] B.Andersson, G.Gustavson, B.Söderberg, Z. Phys. **C20** (1983) 317; M.G.Bowler, Z. Phys. **C11** (1981) 169; D.A.Morris, Nucl. Phys. **B313** (1989) 634.

[5] ALEPH collaboration, D.Buskulic et al., Z. Phys **C62** (1994) 179.

[6] DELPHI collaboration, P.Abreu et al., "Measurement of $\frac{\Gamma_{b\bar{b}}}{\Gamma_{had}}$ using impact parameter measurements and lepton identification", CERN-PPE/95-08

[7] L3 collaboration, O.Adeva et al., Phys. Lett. **B261** (1991) 177.

[8] OPAL collaboration, R.Akers et al., Z. Phys **C60** (1993) 199.

[9] L3 collaboration, O.Adriani et al., Phys. Lett. **B288** (1992) 412.

[10] OPAL collaboration, R.Akers et al., Z. Phys **C61** (1994) 209.

[11] DELPHI collaboration, P.Abreu et al., Z. Phys **C57** (1993) 181.

[12] ALEPH collaboration, D.Decamp et al., Nucl. Instr. Meth. **A294** (1990) 121.

[13] ALEPH collaboration, D.Decamp et al., Nucl. Instr. Meth. **A360** (1995) 481.

[14] ALEPH collaboration, D.Buskulic et al., Nucl. Instr. Meth. **A346** (1994) 461.

[15] JADE collaboration, S.Bethke et al.,Phys. Lett. **B213** (1988) 235.

[16] G.Batignani et al., IEEE Transactions on Nuclear science, **39** (1992) 701.

[17] ALEPH collaboration, D.Buskulic et al., Phys. Lett. **B295** (1992) 174.

[18] ALEPH collaboration, D.Buskulic et al., Phys. Lett. **B313** (1993) 535

[19] ALEPH collaboration, D.Buskulic et al., Phys. Lett. **B295** (1992) 174. Phys. Lett. **B307** (1993) 194-208

[20] ALEPH collaboration, D.Buskulic et al., Phys. Lett. **B322** (1994) 275

[21] B.Anderson, G.Gustavson, G.Ingelman, T.Sjöstrand, Phys. Rep. **97** (1983) 31.

[22] T.Sjöstrand, Computer Physics Commun. **82** (1994) 74. and CERN-TH/93.

[23] ARGUS collaboration, Z. Phys **C57** (1993) 533-540

[24] CLEO collaboration, B.Barish et al., Phys.Rev. **D51** (1995) 1014

[25] ALEPH collaboration, D.Buskulic et al., Phys. Lett. **B345** (1995) 103.

[26] OPAL collaboration, R.Akers et al., " A Study of Charm Meson Production in Semileptonic B Decays ", prep. CERN-PPE/95-02 *(to be published in Z. Phys.C)*

[27] ALEPH collaboration, D.Buskulic et al., Z. Phys **C55** (1992) 209.

[28] G.Marchesini et al., Computer Physics Commun. **67** (1992) 465.

[29] ALEPH collaboration, D.Buskulic et al., "Production of Excited Beauty states in Z decays", CERN-PPE/95-108, *(submitted to Z. Phys. C).*

[30] L3 collaboration, M.Acciari et al., Phys. Lett. **B345** (1995) 589.

[31] DELPHI collaboration, P.Abreu et al., "Observation of orbitally excited B mesons", CERN-PPE/94-210 *(to be published in Phys. Lett. B)*

[32] OPAL collaboration, R.Akers et al., " Observations of $\pi-$B charge-flavor correlations and resonant Bπ and BK production", CERN-PPE/94-206 *(to be published in Z. Phys.C).*